Isoscalar pairing correlations by the tensor force in the ground states of ^{12}C, ^{16}O, ^{20}Ne, and ^{32}S nuclei

Eunja Ha[*]

Department of General Education for Human Creativity, Hoseo University, Asan, Chungnam 336-851, Korea

Seonghyun Kim[†] and Myung-Ki Cheoun [‡]

Department of Physics and Origin of Matter and Evolution of Galaxy (OMEG) Institute, Soongsil University, Seoul 156-743, Korea

H. Sagawa[§]

RIKEN, Nishina Center for Accelerator-Based Science, Wako 351-0198, Japan
and Center for Mathematics and Physics, University of Aizu, Aizu-Wakamatsu, Fukushima 965-8560, Japan

We investigate roles of the tensor force (TF) on the pairing correlations in the ground-state structure of ^{12}C, ^{16}O, ^{20}Ne, and ^{32}S nuclei within a deformed BCS model. For pairing matrix elements, we exploit the Brueckner G matrix derived from the charge-dependent Bonn potential. In particular, the isoscalar (IS) neutron-proton (np) pairing is studied in detail in relation to spin-triplet even TF in the nucleon-nucleon interaction. Detailed analyses of the np pairing and possible enhancement of the IS channel are performed by focusing on roles of attractive spin-triplet even and repulsive spin-triplet odd channels in the TF for the ground states of the nuclei with some deformation. It is also shown that the TF may play a crucial role of properly interpreting the experimental data of a two-nucleon knockout reaction from ^{12}C.

I. INTRODUCTION

Pairing interactions in nuclei are one of the important residual interactions in the mean-field approach for understanding nuclear structure [1]. They have been introduced for studying not only the nuclear collective motion [2] but also the nuclear superfluidity in finite nuclei, and they have been intensively discussed in many reports [3,4]. The correlations by the pairing interactions are also pointed out to play an important role of explaining high-momentum distribution of nucleons beyond Fermi momentum. However most of the distributions are claimed to be closely associated with the short-range correlations [5,6], which are thought to result from the Pauli exclusion principle of two nucleons inside nuclei beyond the mean-field approach [7].

In the present work, we discuss the pairing correlations originated from the nucleon-nucleon (N-N) force, by which the Bardeen-Cooper-Schrieffer (BCS) pairing as well as the Bose-Einstein condensation (BEC) pairing may occur inside nuclei. In practice, the difference between the BEC pairing and the BCS pairing may be studied by the relative distance between the two nucleons in a coordinate space. The coupling strength between them might be the order parameter, which may depend on the density and/or the chemical potential.

In the halo nuclei which have a long low-density tail, as argued by Hagino *et al.* [8] through the calculation of the two-(valence)neutron wave function in ^{11}Li, the BCS-type pairing shows up in the inner side of the nucleus, while the BEC-type pairing may appear near the surface of the halo nucleus. The different phases are thought to stem from the long tail of the density peculiar to the halo nuclei. It infers that the strong pairing interaction at lower density may give rise to the BEC phase or the crossover between the BCS and BEC phases.

We also study the feasibility of the BEC phase by effectively enlarging the isoscalar (IS) pairing strength. But the results do not show any significant indication of the BEC feature, which is expected to come from the fact that density distributions of the $N = Z$ nuclei do not have such a long tail as the halo nuclei. The BEC and BCS phases by neutron-proton interactions have been claimed to be able to manifest themselves in the heavy ion collision (HIC) because of the high temperature and high density expected in the HIC environment [9].

Hereafter, we focus on the BCS-type pairing induced by the tensor force (TF) considering some nuclear deformation. One expects two types of the pairing interactions, like-pairing from neutron-neutron (nn) interaction and proton-proton (pp) interaction and unlike-pairing from neutron-proton (np) interaction. The like-pairing has only an isovector ($T = 1$) channel, while the unlike-pairing has both isovector (IV) and isoscalar (IS) modes. Most study of the pairing correlations have presumed the IV spin-singlet ($S = 0$) state by spin antialigned coupling ($\alpha\bar{\alpha}$) like the Cooper pair, where $\bar{\alpha}$ is the time conjugate state to a particle state α.

---

[*]ejha@hoseo.edu

[†]kimsh@ssu.ac.kr

[‡]Corresponding author: cheoun@ssu.ac.kr

[§]sagawa@ribf.riken.jp

TABLE I. IV and IS pairing scheme by spin-antialigned $(\alpha\bar{\alpha})$ and spin-aligned $(\alpha\alpha)$ and $(\bar{\alpha}\bar{\alpha})$ pairs for like- and unlike-pairing interactions in the (S, L, J, T) scheme. The deuteron ground state $(J^\pi = 1^+, T = 0)$ is composed of $(S, L, J, T) = (1, 0, 1, 0) = {}^3S_1$ and $(1, 2, 1, 0) = {}^3D_1$ configurations in the last row. The projection K of the total angular momentum on the intrinsic symmetry axis is fixed as $K = 0$ for the pairing matrix elements used in this work.

Types	T	S	L	J $(K = 0)$
Like	$T = 1$	$(\alpha\bar{\alpha})$ $S = 0$	$L = 0, 2, 4 \ldots$ (E)	$J = $ Even
		$(\alpha\bar{\alpha})(\alpha\alpha)(\bar{\alpha}\bar{\alpha})$ $S = 1$	$L = 1, 3, 5 \ldots$ (O)	$J = $ Even
Unlike	$T = 1$	$(\alpha\bar{\alpha})$ $S = 0$	$L = 0, 2, 4 \ldots$ (E)	$J = $ Even
		$(\alpha\bar{\alpha})(\alpha\alpha)(\bar{\alpha}\bar{\alpha})$ $S = 1$	$L = 1, 3, 5 \ldots$ (O)	$J = $ Even
	$T = 0$	$(\alpha\bar{\alpha})$ $S = 0$	$L = 1, 3, 5 \ldots$ (O)	$J = $ Odd
		$(\alpha\bar{\alpha})(\alpha\alpha)(\bar{\alpha}\bar{\alpha})$ $S = 1$	$L = 0, 2, 4 \ldots$ (E)	$J = $ Odd

In fact, main contributions of the pairing are believed to come from the IV spin-singlet ($T = 1, S = 0, J = $ even) state and the IS spin-singlet ($T = 0, S = 0, J = $ odd) state in the $(\alpha\bar{\alpha})$ coupling scheme, whose main contributions come from $J = 0$ and $J = 1$ coupling, respectively [10,11]. In particular, because the $J = 0$ coupling is stronger than the $J = 1$ coupling in the $(\alpha\bar{\alpha})$ scheme, in the ground states of $N \simeq Z$ nuclei, the IS spin-singlet np pairing has been thought to be weaker than the IV spin-singlet pairing.

However, if we allow spin-aligned coupling, $(\alpha\alpha)$ and $(\bar{\alpha}\bar{\alpha})$, the IS np pairing may have a spin-triplet state as recapitulated in Table I. The like-pairing with the spin-aligned pairs with $J = $ odd configurations is also plausible, but it is not allowed by the Pauli principle of fermions. Likewise, the unlike IV pairing with the spin-aligned coupling ($T = 1, S = 1$) is possible, but no empirical evidence is found in $N = Z$ nuclei. As a matter of fact, for $N = Z$ nuclei (even for odd-odd $N = Z$ nuclei), the ground state has mostly $S = 0$ states apart from some exceptional cases in $f_{7/2}$ shell nuclei and ^{34}Cl [12]. Therefore, in the present work for ^{12}C, ^{16}O, ^{20}Ne, and ^{32}S nuclei, we focus on the unlike IS spin-triplet ($T = 0, S = 1$) mode, which is closely related to the TF through the spin-triplet $L = $ even coupling.

The TF in the nucleon-nucleon (N-N) interaction is an inevitable ingredient for understanding various nuclear correlations in finite nuclei and also nuclear matter. For example, deuteron ($J^\pi = 1^+, T = 0$) might never be bound without the TF. Lots of phase shift analyses of the N-N scattering data show that the spin-triplet even TF for the $^3S_1$ state is strongly attractive, while it is repulsive for the $^3D_1$ state. This feature was also confirmed from the TF potential by the lattice QCD [13]. Effects of the TF inside nuclei have been extensively studied by many theoretical nuclear models and experimental data during the past 20 years [14–16].

Recently many studies concerning the roles of the TF inside nuclei demonstrated that the tensor interaction is attractive for the particles located in $j_< = l - 1/2$ and $j_> = l + 1/2$ states, while it is repulsive for those in $j_{>(<)}$ and $j_{>(<)}$ states [17,18]. On the other hand, in deformed nuclei, because the total angular momentum $j = l + s$ is not a good quantum number due to the rotational symmetry breaking, the

single-particle state is prescribed by the quantum numbers in the intrinsic frame; the projections of the orbital angular momentum Λ, spin Σ, and total angular momentum $\Omega = \Lambda + \Sigma$. These quantum numbers specify the orbits in the Nilsson model. Within this scheme, we discuss how the deformation of nuclei may influence the pairing properties induced by the TF inside nuclei and vice versa [19].

Along this line, many important experiments for directly searching the TF effect in nuclei have recently been performed, which disclosed quite intriguing results for understanding the pairing correlations inside nuclei. For example, Ref. [20] exhibited that the TF can manifest itself by the deuteron detection in the $(p, p'd)$ reaction at 392 MeV on an ^{16}O target through the neutron pickup process from the deuteron structure inside nuclei. They found a strong population of the $J = 1, T = 0, S = 1$ state at 3.95 MeV by the TF and a very weak population of the $J = 0, T = 1, S = 0$ state at 2.31 MeV. These states are observed by the cross sections for the excitations of ^{14}N, whose $J^\pi = 1^+$ ground state has two transitions with the multiplicities $L = 2$ and 0. This implies the presence of the IS spin-triplet unlike-pairing correlations. Consequently it may infer that the deuteron structure may exist with a certain probability inside the nucleus and its existence can be studied through the neutron pickup reaction by the incident energetic proton. Not only proton beams but also electron beams are also feasible for looking for the deuteron ejection related to the TF inside nuclei as suggested in Refs. [5,6,21]. However, the high-momentum density by the short-range correlations is about four times smaller than the main peak of the momentum density distribution, which makes it difficult to detect the deuteron itself by the high energetic electron or proton [18].

For the past decade, a lot of effort has also been paid to finding some evidence of the unlike-pairing correlations in $N = Z$ nuclei because one expects a strong overlap of neutron and proton wave functions in $N \sim Z$ nuclei. For example, in Ref. [22] it is argued that some heavy $N = Z$ nuclei around the $60 < N < 70$ and $57 < Z < 64$ region may have IS pairing dominance or coexistence with IV pairs. Our previous papers [23,24] have discussed that some sd- and pf-shell $N \sim Z$ nuclei may have such IS dominance for some specific deformation cases and have demonstrated that enhanced IS pairing may induce the IS condensation in some deformed $N = Z$ nuclei. Furthermore, recent data of the spin-$M1$ excitation [25] has shown that the IV contribution may be strongly quenched, and consequently the IS pairing correlations could be enhanced in sd-shell $N = Z$ nuclei. However, the relationship between the IS pairing interactions induced by the TF and the deformation seems to be not discussed enough. In the present work, we study the competition of IS and IV pairing interactions induced by the TF and also the deformation effect on the pairing correlations in detail.

This paper is organized as follows. Section II is devoted to the basic formalism of the deformed BCS theory including both IS and IV pairing interactions. Results of the TF effects in ^{12}C, ^{16}O, ^{20}Ne, and ^{32}S nuclei are discussed in Sec. III. The TE effect in the two-nucleon knockout reaction from ^{12}C is calculated in Sec. IV and compared with the available experimental data. A summary and conclusions are given in Sec. V.

II. BASIC FORMULA

In this work, we take the Goswami and Kisslinger formalism for the pairing interaction in a deformed BCS approach (DBCS) [26] and focus on the unlike-pairing correlations retaining high angular momentum. Because the theoretical framework for the DBCS approach has already been detailed in our previous papers [23,24], we present only the basic formula. We start from the following DBCS transformation between a quasiparticle and a real particle in an α state:

$$
\begin{pmatrix} a_1^\dagger \\ a_2^\dagger \\ a_{\bar 1} \\ a_{\bar 2} \end{pmatrix}_\alpha = \begin{pmatrix} u_{1p} & u_{1n} & v_{1p} & v_{1n} \\ u_{2p} & u_{2n} & v_{2p} & v_{2n} \\ -v_{1p} & -v_{1n} & u_{1p} & u_{1n} \\ -v_{2p} & -v_{2n} & u_{2p} & u_{2n} \end{pmatrix}_\alpha \begin{pmatrix} c_p^\dagger \\ c_n^\dagger \\ c_{\bar p} \\ c_{\bar n} \end{pmatrix}_\alpha , \quad (1)
$$

where u and v coefficients are calculated by the following 4×4 DBCS equation:

$$
\begin{pmatrix} \epsilon_p - \lambda_p & 0 & \Delta_{p\bar p} & \Delta_{p\bar n} \\ 0 & \epsilon_n - \lambda_n & \Delta_{n\bar p} & \Delta_{n\bar n} \\ \Delta_{p\bar p} & \Delta_{p\bar n} & -\epsilon_p + \lambda_p & 0 \\ \Delta_{n\bar p} & \Delta_{n\bar n} & 0 & -\epsilon_n + \lambda_n \end{pmatrix}_\alpha \begin{pmatrix} u_{\alpha'' p} \\ u_{\alpha'' n} \\ v_{\alpha'' p} \\ v_{\alpha'' n} \end{pmatrix}_\alpha
$$
$$
= E_{\alpha\alpha''} \begin{pmatrix} u_{\alpha'' p} \\ u_{\alpha'' n} \\ v_{\alpha'' p} \\ v_{\alpha'' n} \end{pmatrix}_\alpha . \quad (2)
$$

Here $E_{\alpha\alpha''}$ is an energy of the quasiparticle $\alpha''(=1, 2)$ in the α state. We include $n\bar p$ and $\bar n p$ pairings in addition to the like-pairing ($p\bar p$ and $n\bar n$) correlations. The pairing potentials Δ in Eq. (2) are permitted between the nucleons in a time-reversed state ($\alpha\bar\alpha$) [27]. The unlike-pairing may have ($\alpha\alpha$) pairing as well as ($\bar\alpha\bar\alpha$) pairing [28], which are effectively included in the present framework as discussed later on. For the mean field we take a deformed Woods-Saxon potential [29] for its simplicity. The self-consistent mean field by the deformed Hartree-Fock-Bogoliubov approach is in progress.

In the DBCS approach, the conventional quasiparticle is mixed with a particle state and its hole state. In the present framework, the quasiparticle is also mixed with additional couplings of proton and neutron by the np pairing. Furthermore the quasiparticle state is additionally mixed with different single-particle states because each deformed state is represented by a linear combination of the spherical states (see Ref. [19] and Fig. 1 at Ref. [30]) up to higher j single-particle states with the fixed projected value $\Omega = 0$ on the symmetry axis. This feature is one of extra features due to the inclusion of deformation in the DBCS approach.

The pairing potentials in Eq. (2) are calculated in the deformed basis by using the Brueckner G matrix derived from the realistic charge-dependent (CD) Bonn potential, which explicitly employed the TF through the pion and ρ-meson exchange in the one-boson-exchange potential (OBEP) for the N-N interaction, in the following way:

$$
\Delta_{p\bar p_\alpha} = \Delta_{\alpha p\bar\alpha p} = -\sum_\gamma \left[\sum_{J,a,c} g_p F_{\alpha a\bar\alpha a}^{J0} F_{\gamma c\bar\gamma c}^{J0} G(aacc, J, T=1) \right]
$$
$$
\times \left(u_{1p_\gamma}^* v_{1p_\gamma} + u_{2p_\gamma}^* v_{2p_\gamma} \right), \quad (3)
$$

$$
\Delta_{p\bar n_\alpha} = \Delta_{\alpha p\bar\alpha n}
$$
$$
= -\sum_\gamma \left\{ \left[\sum_{J,a,c} g_{np}^{T=1} F_{\alpha a\bar\alpha a}^{J0} F_{\gamma c\bar\gamma c}^{J0} G(aacc, J, T=1) \right] \right.
$$
$$
\times \mathrm{Re}\left(u_{1n_\gamma}^* v_{1p_\gamma} + u_{2n_\gamma}^* v_{2p_\gamma} \right)
$$
$$
+ \left[\sum_{J,a,c} g_{np}^{T=0} F_{\alpha a\bar\alpha a}^{J0} F_{\gamma c\bar\gamma c}^{J0} iG(aacc, J, T=0) \right]
$$
$$
\left. \times \mathrm{Im}\left(u_{1n_\gamma}^* v_{1p_\gamma} + u_{2n_\gamma}^* v_{2p_\gamma} \right) \right\}, \quad (4)
$$

where $F_{\alpha a\bar\alpha a}^{JK} = B_a^\alpha B_a^{\bar\alpha} C_{j_a \Omega_\alpha j_a - \Omega_\alpha}^{JK} (K = \Omega_\alpha - \Omega_{\bar\alpha})$ was introduced to take into account the deformation in the G matrix with an expansion coefficient B_α [30] from the deformed single-particle state (SPS):

$$
B_a^\alpha = \sum_{N n_z \Sigma} C_{l\Lambda \frac{1}{2}\Sigma}^{j\Omega_\alpha} A_{N n_z \Lambda}^{N_0 l} b_{N n_z \Sigma}, \quad A_{N n_z \Lambda}^{N_0 l} = \langle N_0 l \Lambda | N n_z \Lambda \rangle. \quad (5)
$$

Detailed formulas used for the coefficient B_a^α and the overlap integral $A_{N n_z \Lambda}^{N_0 l}$ of the deformed and spherical state are presented in Ref. [19]. The $T = 0$ pairing contribution is included as an imaginary term in the np pairing potential in Eq. (4). K is a projection number of a total angular momentum J onto the intrinsic symmetry axis and selected as $K = 0$. The Brueckner $G(aacc\, JT)$ matrix represents the state-dependent pairing matrix elements (PMEs) calculated in the spherical basis. We sum up all possible J values in the coupling for a two-particle state assigned by (aa) or (cc) in the spherical basis, which has the $K = 0$ projection state. This sum of the J value is due to the expansion of the deformed state by the spherical states (aa) or (cc). $\Delta_{\alpha n\bar\alpha n}$ is obtained from Eq. (3) by replacing p by n.

Here, we note that higher angular momentum components of the pairing correlations are included in the present scheme. For example, for the like-pairing, the IV state may have only $S = 0$, $L =$ even components by the antisymmetric property of fermions. The unlike-pairing gaps have both IS and IV components and each component may have $S = 0$ as well as $S = 1$ components, which are coupled to the angular momentum L with the antisymmetric condition.

As for the IS np pairing, we have two modes, spin-singlet ($S = 0$) and spin-triplet ($S = 1$). In particular, the $S = 1$ state comes from the ($\alpha\alpha$) and ($\bar\alpha\bar\alpha$) pairings. In fact, we need the extended pairing scheme due to the ($\alpha\alpha$) and ($\bar\alpha\bar\alpha$) components, which requires an 8×8 transformation matrix instead of Eq. (2) [31]. Within the present 4×4 scheme, in which we included only $n\bar p$ and $\bar p n$ pairing correlations, we effectively take into account the $T = 0$ channel by the ($\alpha\alpha$) and ($\bar\alpha\bar\alpha$) coupling to the $T = 0$ pairing matrices in the ($\alpha\bar\alpha$) configuration in the following way. By adopting the procedure in Ref. [31], for np and $\bar n\bar p$ pairings, we assume

$$
\langle \alpha n\alpha p, T = 0 | V_{\mathrm{pair}} | \beta n\beta p, T = 0 \rangle
$$
$$
= \langle \alpha n\alpha p, T = 0 | V_{\mathrm{pair}} | \bar\beta n\bar\beta p, T = 0 \rangle. \quad (6)
$$

TABLE II. Deformation parameters β_2^{E2} from the experimental $E2$ transition data [32] are given as their absolute values. The theoretical β_2 by relativistic mean-field (RMF) theory [33] and finite-range droplet model (FRDM) model [34] and $Q_{\text{exp.}}$ from experimental data [35] are also tabulated for ^{12}C, ^{16}O, ^{20}Ne, and ^{32}S nuclei. Empirical pairing gaps deduced from the five-point mass formula [36] are also shown. The deformation of ^{12}C was predicted as oblate in Ref. [37], but the experimental ^{12}C + ^{12}C scattering data showed both deformation possibilities [38].

Nucleus	β_2^{E2} [32]	β_2^{RMF} [33]	β_2^{FRDM} [34]	$Q_{\text{exp.}}$ (barn) [35]	Δ_p^{emp}	Δ_n^{emp}	Δ_{np}^{emp}
^{12}C	$\|0.582\|$	–	–	$+0.06(3)$	4.430	4.547	2.489
^{16}O	$\|0.364\|$	–	-0.01	–	3.538	3.672	1.761
^{20}Ne	$\|0.562\|$	0.186	0.364	$-0.23(3)$	3.592	3.630	2.585
^{32}S	$\|0.312\|$	0.186	0.221	$-0.12(5)$ to $-0.18(4)$	2.141	2.207	1.047

Then the $\Delta_{\alpha n \alpha p}^{T=0}$ pairing potential is given as Im $\Delta_{\alpha n \alpha p}^{T=0} = 0$ and Re $\Delta_{\alpha n \alpha p}^{T=0} = \text{Im} \Delta_{\alpha n \bar\alpha p}^{T=0}$ by Eqs. (5)–(7) in Ref. [31]. It leads to

$$\Delta_{np}^{2\ (T=0)} = 2\left|\Delta_{\alpha p \bar\alpha n}^{T=0}\right|^2 + 2\left|\Delta_{\alpha p \alpha n}^{T=0}\right|^2 = 4\left|\Delta_{\alpha p \bar\alpha n}^{T=0}\right|^2, \quad (7)$$

where a factor 2 is due to $\bar\alpha p \alpha n$ and $\bar\alpha p \bar\alpha n$ pairings, respectively. Consequently, we multiply by a factor 2 on the $T = 0$ PMEs in Eq. (4).

The strength parameters $(g_p, g_n, g_{np}^{T=1})$ in Eqs. (3) and (4), which are a kind of the renormalization constant due to the finite Hilbert particle model space, are fitted to reproduce the empirical pairing gaps in Table II evaluated by the odd-even mass difference. For the IS ($T = 0$) enhancement, we introduce the strength parameter $g_{np}^{\text{eff}} = 1.0$–$1.3$, which is multiplied as $g_{np}^{T=0} = g_{np}^{T=1} \times 2 \times g_{np}^{\text{eff}}$. Here the factor 2 comes from Eq. (7).

III. RESULTS

In the following, we discuss the IV and IS np pairings in ^{12}C, ^{16}O, ^{20}Ne, and ^{32}S. Specifically, we investigate the contribution of the TF to the np pairing, which results mainly from the IS spin-triplet np coupling. First, we estimate the ratio of the IV (IS) contribution to the total np pairing gap for ^{12}C in terms of the deformation parameter β_2, which is given as a complex number as shown in Eq. (4),

$$\Delta_{\text{total}} = \Delta_{\text{IV}} + i\Delta_{\text{IS}}, \quad (8)$$

and calculated by subtracting the total energy of the system without np pairing from that with np pairing using an iteration method for the DBCS Eq. (2) to fit the empirical pairing gaps in Table II [30].

The results for the IV pairing are calculated by summing J = even states with the projection $K = \Omega_\alpha - \Omega_{\alpha'} = 0$. For the IS spin-singlet and spin-triplet we take a summation for the J = odd state. The TF is explicitly included in the IS spin-triplet as argued below.

Before showing numerical results for the IS pairing, we briefly explain how to separate the TF effect in the G matrix calculated from the CD Bonn potential. The TF stems from the pion and ρ-meson exchange potentials, whose detailed discussions can be found in Refs. [39,40]. Because the TF is not accommodable well in the j-j coupling scheme [41], we exploit the N-N potential represented by the L-S coupling scheme, $|LSJM\rangle$ basis [39], which further makes it easy to apply the G matrix to the PMEs. The N-N potential comprising each meson-exchange potential is decomposed by

spin-singlet, uncoupled spin-triplet and coupled spin-triplet channels, where the last one corresponds to the TF comprising $\Delta L = 2$ and $\Delta L = 0$ components [40]. One can easily show that the coupled spin-triplet L = even potential is fully associated with the deuteron wave function. Inside nuclei, not only $J = 1$ but also other J coupling TFs play significant roles. Other mesons besides pion and ρ meson do not contribute to the spin-triplet potential, which can be confirmed in the Bonn potential code [40].

In Fig. 1, we present the TF effect on the pairing gaps by switching on and off its contribution to the PMEs. The black open squares and the red open circles in Fig. 1(a) are calculated without the TF and illustrate that the IV pairing could dominate the np pairing correlations without the TF. The TF presented by the black squares and the red circles breaks more or less the IV dominance over the IS pairing with the increase of the prolate deformation. We can confirm in Fig. 1(a) that the TF effect directly increases the IS np pairing, although the IV contribution is still larger than the IS one. Because the total gaps, Δ_{total}, are fitted to empirical data at each deformation, the IV pairing gaps are changed together with the change of IS values when the TF is switched on.

In a nutshell, with the increase of the deformation, the IS spin-triplet tensor contribution to the np pairing increases. In particular, beyond $\beta_2 > 0.3$ the IS contribution amounts to 20% of the IV in ^{12}C. It implies that the TF contribution in the IS channel is sensitive to the evolution of the SPS by the deformation. In the oblate-deformed region, the TF effect does not change the ratio of the IV to the IS pairing gap much; therefore, we do not show the results.

Numbers of nn, pp, and np pairs are presented for the case including and excluding the TF, respectively, in Fig. 1(b). They are calculated by the expectation value of the following number operators of the pairs [42],

$$\mathcal{N}_{pp} = \sum_{s,s'} S_{spp}^{T=1\dagger} S_{s'pp}^{T=1}, \ \mathcal{N}_{nn} = \sum_{s,s'} S_{snn}^{T=1\dagger} S_{s'nn}^{T=1},$$

$$\mathcal{N}_{np} = \sum_{s,s'} \left(S_{snp}^{T=1\dagger} S_{s'np}^{T=1} + S_{snp}^{T=0\dagger} S_{s'np}^{T=0}\right), \quad (9)$$

with

$$S_{s\rho\rho}^{T=1\dagger} = \sum_\sigma c_{\rho s \sigma}^\dagger c_{\rho s \bar\sigma}^\dagger,$$

$$\S_{s\rho\rho'}^{T=1(0)\dagger} = \sum_\sigma \frac{1}{\sqrt{2}}(c_{\rho s \sigma}^\dagger c_{\rho' s \bar\sigma}^\dagger + (-)c_{\rho' s \sigma}^\dagger c_{\rho s \bar\sigma}^\dagger), \quad (10)$$

where $c_{\rho\sigma s}^+$ is the real particle creation operator in the axially symmetric harmonic oscillator potential. The single-particle
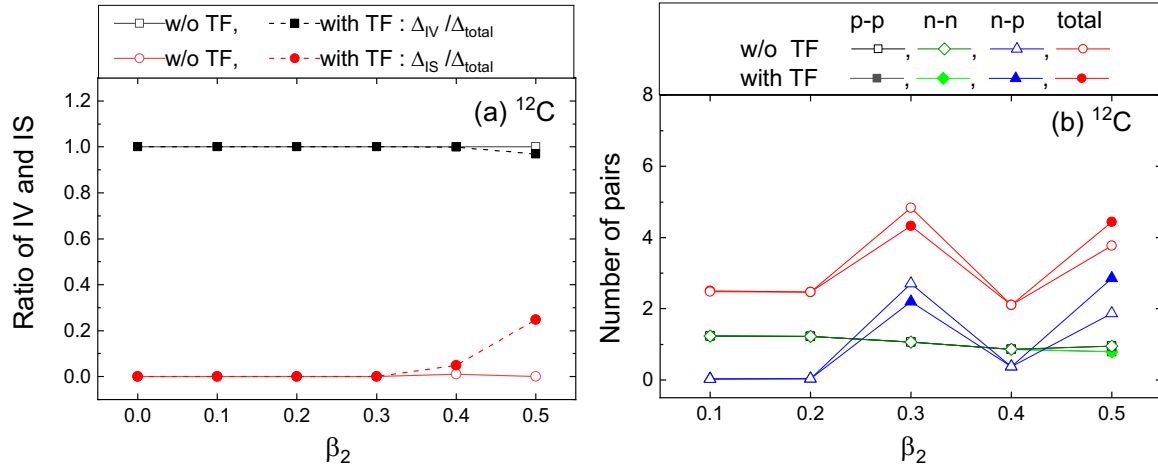
FIG. 1. (a) Ratio of IV and IS pairing gap to the total np pairing gap by Eq. (4) for ^{12}C. Black (open) squares and red (open) circles are IV and IS ratios to the toal np pairing gap, respectively, with (without) the TF, which are denoted as with TF (w/o TF). Here $\Delta_{\text{total}} = \sqrt{|\Delta_{\text{IV}}|^2 + |\Delta_{\text{IS}}|^2}$. (b) Number of pairs by Eq. (9). Like pairings for p-p and n-n and unlike pairing for the n-p pair are denoted as the black (open) squares, green (open) diamonds, and blue (open) triangles with (without) TF. Both like pairings are almost degenerate and indistinguishable. The total number of pairs are presented as red circles in a similar fashion.

states (SPSs) are completely determined by a principal set of quantum numbers: $s = [N, n_z, \Lambda, \Omega]$. The σ is a sign of the angular momentum projection $\Omega (\sigma = \pm 1)$. The ρ and ρ' specify the isospin quantum number for the SPSs specified by a set of quantum numbers s.

The numbers of nn and pp pairs in Fig. 1(b) are rarely affected by the TF, while the number of np pairs changes at a certain nuclear deformation. This feature stems from the shell evolution with the deformation and the intrinsic nature of the TF. There are big changes in the number of np pairs at $\beta_2 = 0.3$ and 0.5. At $\beta_2 = 0.3$, the np pair is entirely due to the IV pair because there is no IS pairing gap in Fig. 1(a). On the other hand, at $\beta_2 = 0.5$, we see that both IS and IV np pairs coexist because the IS pairing gap is raised Fig. 1(a). That is, the TF affects the pairing correlations and the numbers of pairs in a different way in each IS and IV channel. In general, the spin-triplet even TF has a strong attractive nature for the $T = 0$ state ($^3S_1$, $^3D_2$, and $^3D_3$), while the spin-triplet

odd TF is repulsive in $T = 1$ channels like $^3P_1$. These different behaviors of the IV and IS channels of the TF give rise to various changes in the pairing gaps and the number of pairs in the nuclei discussed below.

In brief, for ^{12}C, the TF increases (decreases) the PMEs of the $T = 0$ np channel by its attractive (repulsive) property around the $\beta_2 \approx 0.5(0.3)$ region. The nn and pp pairs may be affected by the TF. The effect, however, is very small as shown in black square and green diamond symbols, which are almost degenerate. Detailed TF effects in the PMEs are explained further in Fig. 4.

Figure 2 shows the results for ^{16}O, which is a double closed shell nucleus. Because ^{16}O was used for the ^{16}O$(p, p'd)^{14}$N reaction experiment [25], we make detailed analyses to figure out the TF effect in the np pairing correlations in the same way as ^{12}C. One interesting point is that the TF effect in the ratio rarely appears contrary to that of ^{12}C even in the $\beta_2 \geqslant 0.3$ region as shown in Fig. 2(a). However, the TF effect in Fig. 2(b)
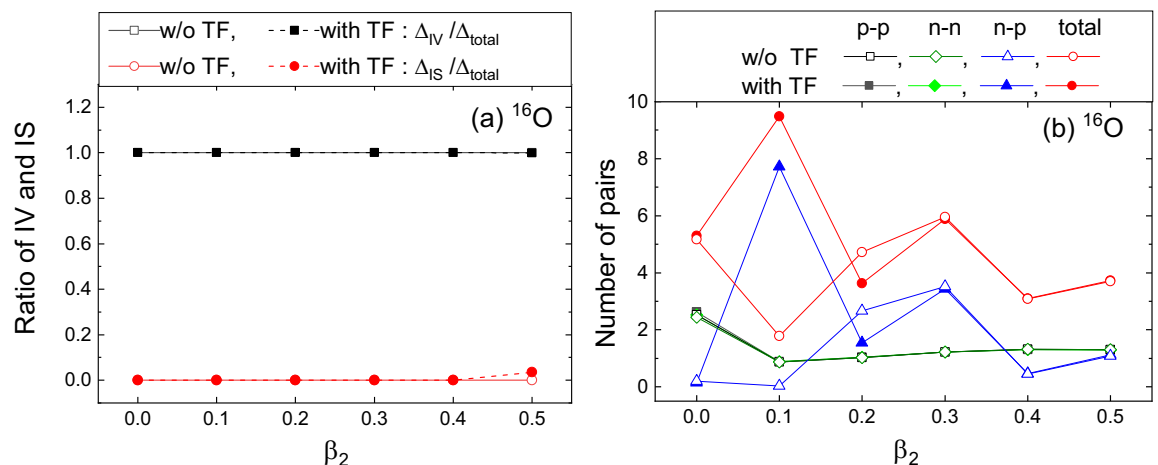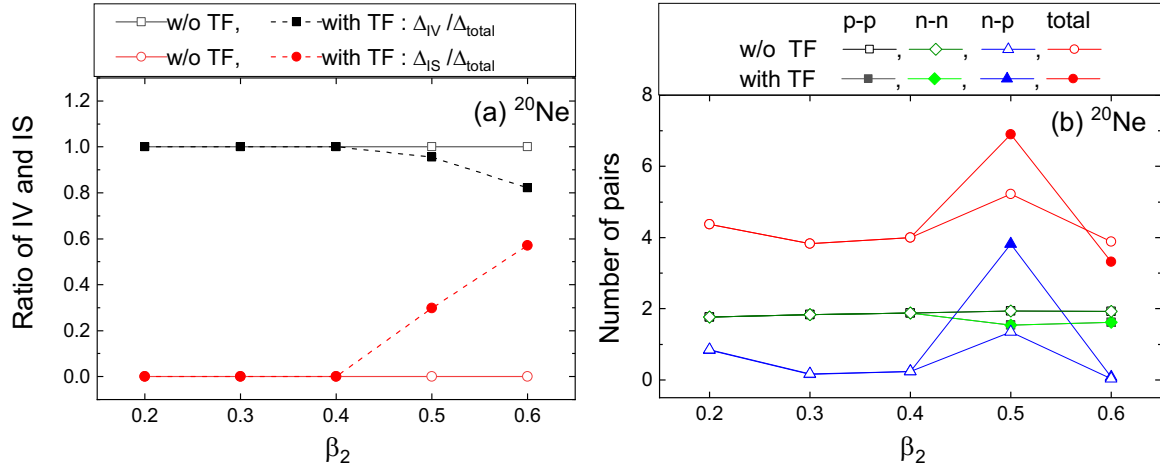

FIG. 2. Same as Fig. 1, but for ^{16}O.

FIG. 3. Same as Fig. 1, but for ^{20}Ne.

appears significantly at the $\beta_2 = 0.1$ and 0.2 deformations, changing the number of the np pairs. Similarly to the ^{12}C case, the change of the number of the np pairs is sensitive to both the TF and the deformation. It means that the TF effect increases (reduces) the np pair number by its attractive (repulsive) property in the $\beta_2 \approx 0.1$ (≈ 0.2) region in Fig. 2(b). Namely, the effect of TF would manifest itself in the number of np pairs if ^{16}O were slightly deformed, about $\beta_2 \approx 0.1$ and 0.2, according to the present calculation. We note that the large quadrupole deformation parameter β_2^{E2} of ^{16}O in Table II does not necessarily mean the shape deformation.

Figure 3 presents the results for ^{20}Ne, where the IS pairing contribution becomes comparable to that of the IV pairing contribution above the $\beta_2 \geqslant 0.4$ region by the attractive TF. This may imply that the IS np pairs can be significantly condensed in ^{20}Ne, if the IS enhancement, likewise ^{24}Mg in the spin-$M1$ excitation data [25,43], takes place in ^{20}Ne. Also as shown in Fig. 3(b), the number of np pairs in ^{20}Ne becomes larger than the numbers of nn and pp pairs by the TF at $\beta_2 = 0.5$. To understand the peculiar property around $\beta_2 = 0.5$, we note that the $0p_{3/2}$, $0p_{1/2}$, and $0d_{5/2}$ states are more or less smeared with the deformation in the deformed Woods-Saxon potential. Because the $0p_{3/2}$ and $0d_{5/2}$ states are $j_> = l + 1/2$ and the $0p_{1/2}$ state is $j_< = l - 1/2$, respectively, the attractive TF may work to create a dense level density around the Fermi surface. For this reason, these single-particle states are smeared further by the pairing interaction, which induces a larger number of np pairs. This TF property gives rise to the $T = 0$ np pair dominance around the Fermi surface.

In Fig. 4, we present the TF effect on the PME; the figure shows a clear TF effect on the $j_>$ and $j_<$ states. For instance, the interactions between the $d_{(5/2)}[\Omega^\pi = (\frac{5}{2})_1^+]$ state and the $d_{(3/2)}[\Omega^\pi = (\frac{3}{2})_2^+]$ state show a large difference due to the TF, where the upper (lower) direction of the arrows in the leftmost circles and the rightmost triangles implies the repulsive (attractive) interaction. Here we also note that the spherical single-particle states no longer have the good quantum numbers l and j, but they are main contributions to the corresponding Nilsson basis used in the present calculation.

In Fig. 5 for the case of ^{32}S, the TF effects become apparent with the increase of the prolate deformation. After the critical deformation $\beta_2 > 0.4$, the IS contribution to the np pairing gap becomes comparable to the IV contribution. The variation of the number of np pairs complies with the IV and IS ratios. This means that the np pair in ^{32}S is almost the IS np pair due to the TF. Around the $\beta_2 \approx 0.0$ region, the TF plays a role in the ratio, but the number of np pairs is only slightly decreased, which may come from a weak repulsive TF or the competition of the repulsive and the attractive TF properties.

Hereafter we discuss the effect of the plausible IS pairing enhancement in $N = Z$ nuclei [25,44,45]. It would be interesting if we could expect the BEC feature inside nuclei from the increase of the IS coupling constant. We increase $g_{np}^{T=0}$
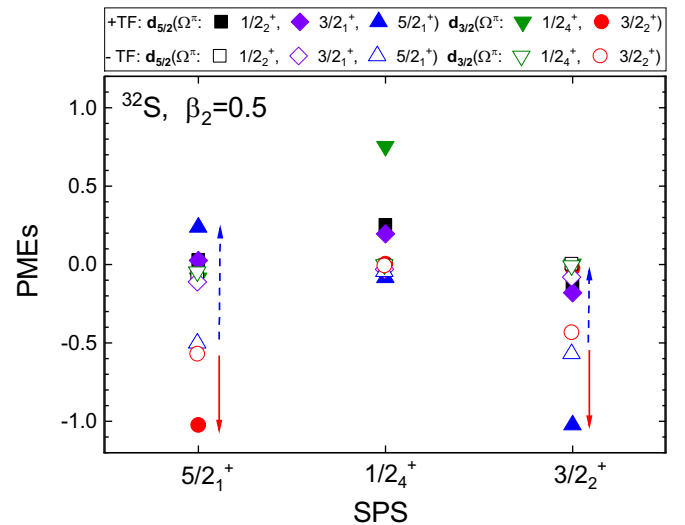

FIG. 4. The TF effects on pairing matrix elements (PMEs) by the G matrix, $G(aacc, J = 1, T = 0)$ in Eq. (4), as a function of the single-particle state (SPS) in the Nilsson basis with and without the TF for ^{32}S at $\beta_2 = 0.5$. The solid (empty) symbols denote the results with (without) the TF. The configurations written below the abscissa correspond to a, while those in the small box are c configurations in the G matrix.
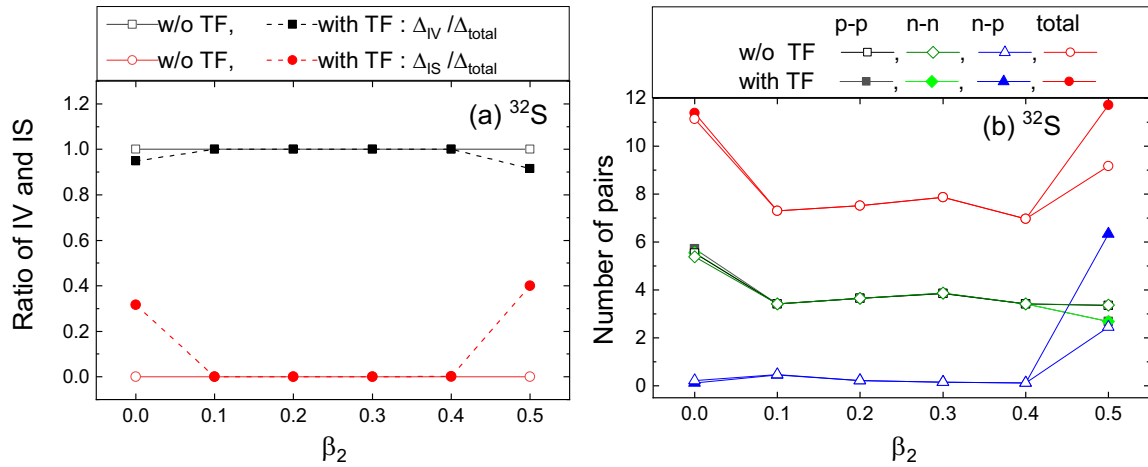
FIG. 5. Same as Fig. 1, but for ^{32}S.

in Eq. (4), by multiplying a factor, g_{np}^{eff}, from 1.0 up to 1.3, to $g_{np}^{T=1}$. Here we note that the g_{np}^{eff} is a kind of theoretical assumption for the test of the crossover phase transition from the BCS phase to the BEC phase. In Fig. 6, we present the number of

pairs in ^{20}Ne for a given deformation β_2 as a function of g_{np}^{eff}. The TF significantly affects the numbers of total and np pairs at $\beta_2 = 0.5$ as shown in Fig. 6(c) by the solid red circles and blue triangles. However, they are not changed so much with
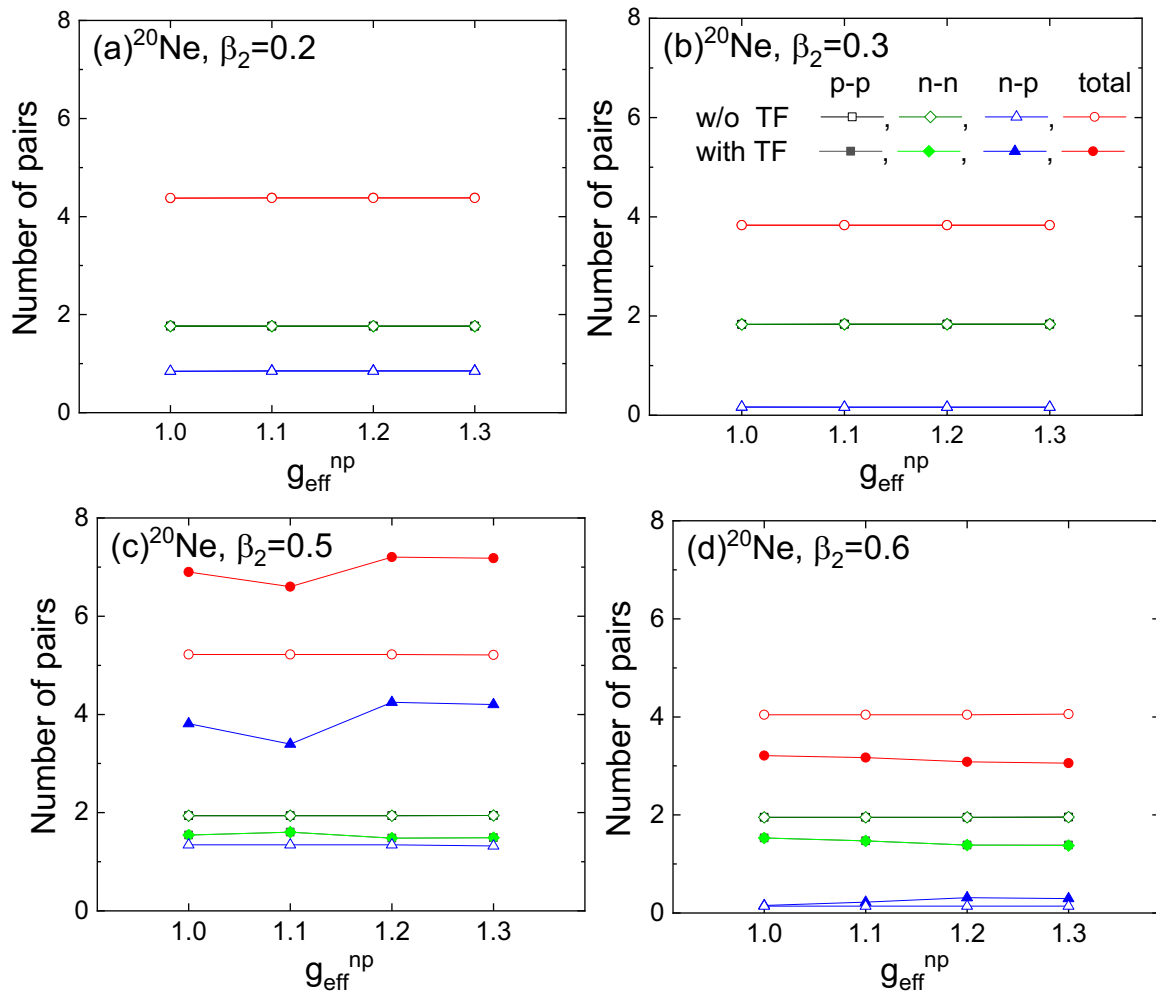

FIG. 6. Number of pairs in terms of the effective np ($T = 0$) coupling strength g_{np}^{eff} for ^{20}Ne. The empirical pairing gaps are fitted for each g_{np}^{eff}. Notations are the same as those in Fig. 1(b).

TABLE III. Ratios of the np knockout to nn and pp knockout cross sections for $^{12}C + ^{12}C$ reactions. Calculated results are given in the last four columns in different deformations with and without the TF (denoted as with TF and without TF) by using the number of pairs in Fig. 1(b) calculated by Eq. (11). Experimental data are taken from Ref. [47].

Ratio	Energy	Exp. data	Without TF $\beta_2 = 0.3$	With TF $\beta_2 = 0.3$	Without TF $\beta_2 = 0.5$	With TF $\beta_2 = 0.5$
$\sigma_{-np}/\sigma_{-nn}$	250 MeV	$47.50/5.33 = 8.91$				
	1.05 GeV	$27.90/4.44 = 6.28$	7.8	4.5	4.0	9.7
	2.1 GeV	$35.10/4.11 = 8.54$				
$\sigma_{-np}/\sigma_{-pp}$	250 MeV	$47.50/5.88 = 8.09$				
	1.05 GeV	$27.90/5.30 = 5.26$	7.8	4.5	4.0	9.7
	2.10 GeV	$35.10/5.81 = 6.04$				

the increase of the IS pairing strength regardless of the TF inclusion. The numbers of pairs are almost saturated even for the larger g_{np}^{eff} cases. This means that the BEC phase might not occur in ^{20}Ne, at least according to the present calculation.

Another remarkable point in Fig. 6(c) is the small change of the nn and pp pairs by the TF. It is originated by the repulsive TF for the isospin-triplet odd channel for the ($J = 0$ and $T = 1$) nn and pp pairs. The present theoretical framework is based on the Nilsson basis, which makes it possible to couple the pair in different single-particle states, by which the isospin-triplet odd TF may contribute.

IV. COMPARISON WITH THE EXPERIMENTAL DATA

Here we discuss whether the TF effects on the numbers of nn, pp, and np pairs can be detected by two-nucleon knockout and/or two-nucleon transfer reaction experiments. In particular, the two-nucleon knockout reactions might be promising experimental probes to observe the feasibility of the BCS and BEC phases in the ground state. The cross section of the two-nucleon knockout reaction is expressed by the following formula [46],

$$\sigma_{\rho\rho'} = \sigma_{\mathrm{unit}} |\mathcal{N}_{\rho\rho'}|^2, \qquad (11)$$

where σ_{unit} is a unit cross section determined by the kinematic conditions of two-nucleon knockout reactions, and the number of pairs $\mathcal{N}_{\rho\rho'}$ is defined in Eq. (9) with $\rho\rho' = pp$, nn, or np pair channels. In the np transfer channel, both $T = 1$ and $T = 0$ couplings are possible, while the pp and nn channels allow only $T = 1$.

Two-nucleon knockout reactions at three different energies of the ^{12}C projectile were performed as $^{12}C + ^{12}C \rightarrow X + Y$, where X stands for ^{10}Be, ^{10}C, and ^{10}B for $Y = pp$, nn, and np pairs, respectively [47]. The measured cross sections of σ_{-pp}, σ_{-nn}, and σ_{-np} are tabulated in Table III. The data were analyzed by using shell-model wave functions presented in Refs. [48,49]. In Ref. [48], a phenomenological interaction is adopted in a large shell-model space, while in Ref. [49] the no-core shell model (NCSM) calculation was performed including three-body interactions. Both calculations reproduced well the σ_{-pp} and σ_{-nn} cross sections, but underestimated the σ_{-np} cross section by about a factor of 2.

We evaluate the ratios of σ_{-np} to σ_{-pp}, and of σ_{-np} to σ_{-nn} by adopting the calculated numbers of pairs in Eqs. (9) to (11). The results are given in Table III with the available experimental data [47]. For the $\beta_2 = 0.5$ (0.3) case, the TF increases (decreases) the ratio, as also shown by the number of pairs in Fig. 1(b). The calculated ratios $\sigma_{-np}/\sigma_{-pp}$ and $\sigma_{-np}/\sigma_{-nn}$ are very sensitive to both the deformation and the TF contribution to the ($T = 0, J = 1$) pairing matrix elements. For a large deformation $\beta_2 = 0.5$, the result with the TF contribution gives a large ratio of 9.7, which is slightly larger than the experimental ratio, but quite acceptable considering the 10–20% experimental uncertainty [47]. The results for the smaller deformation $\beta_2 = 0.3$ case are changed from 7.8 to 4.5 by the TF contribution. These results imply the importance of the TF for understanding the np knockout data. Here we note that the experimental data reveal explicitly energy dependence, specifically, in the σ_{-np} case. In the present work we presumed that the kinematical factor is fully factorized into the σ_{unit} in Eq. (11). More detailed calculations of the two-nucleon knockout reactions beyond Eq. (11) are necessary for more quantitative understanding of the TF effects in the experimental data.

For the $T = 0$ np pair condensation, the np pair transfer reactions $(p, ^3\mathrm{He})$ and $(^3\mathrm{He}, p)$ are also plausible reactions for this study, which have been recently carried out at the Research Center for Nuclear Physics for $N = Z$ nuclei such as ^{24}Mg, ^{28}Si, ^{32}S, and ^{40}Ca [50]. Ayyad et al. [50] compared the ratio of 0^+ and 1^+ cross sections in the residual odd-odd nuclei caused by $T = 1$ and $T = 0$ np pairing excitations, respectively, by taking the forward angular distribution data. They found that, for the cross section to the 1^+ state, $T = 0$ dominates over the ground state of both ^{24}Mg and ^{40}Ca. Also by analyzing the differential cross-section data for $^{24}\mathrm{Mg}(p, ^3\mathrm{He})^{22}$Na, they argued the importance of the $T = 0$ component in the interaction between $d_{5/2}$ and $d_{3/2}$ states, which is closely related to the TF by the spin-aligned triplet state excluded in the typical Cooper pair. To interpret the cross-section ratio of $\sigma(0^+)/\sigma(1^+)$ for the ^{22}Na excitation, where $\sigma(0^+)$ and $\sigma(1^+)$ are presumed to be caused by $T = 1, J = 0$ and $T = 0, J = 1$ np coupling schemes, respectively, we need to do the distorted wave Born approximation (DWBA) calculation including the study of the TF effects in the excitation; we leave that to a future work.

The validity of the BCS model has been scrutinized by Sandulescu and Bertsch [51], who argued clearly the limits of the BCS model by comparing the BCS and number-projected BCS (PBCS) models. The comparisons were done by the

Hartree-Fock calculations in a solvable model, and it was concluded that the BCS is insufficient for properly describing the pairing correlations in light nuclei because of the particle number fluctuation, although the whole results depend on the choice of coupling constant. In the present approach, we exploit a fixing procedure of relevant coupling constants to the empirical pairing gaps by odd-even mass difference to partially cure the problem in the BCS pairing gap. This procedure has been adopted commonly in the study of nuclear structure calculations. However, it has been pointed out that the method does not guarantee the validity of the BCS approximation [51]. A more refined approach like the PBCS approach is preferred to conclude in a quantitative level the number of pairs discussed in the present work. We should consider the present results in a semiquantitative level, but the effect of the TF on the number of pairs could be common in both BCS and PBCS approaches.

We note that *ab initio* calculations for light nuclei as was done in Ref. [52] are more fundamental and successful for describing static nuclear properties. Our previous calculations for the static properties [23,24] using the present Woods-Saxon mean-field approach were not sufficient enough for properly explaining such properties. This problem should also be discussed in future work by using more advanced nuclear models. However, to our knowledge, the relation of the TF and the deformation has not been studied in detail using these *ab initio* calculations. We hope that more extensive study of the nuclear structure will be done in the near future including those effects by the NCSM.

V. SUMMARY AND CONCLUSIONS

In summary, we investigated the TF effect on the np pairing correlations for the ground state of ^{12}C, ^{16}O, ^{20}Ne, and ^{32}S by using a deformed BCS model. The noncentral TF effect turns out to be sensitive to the deformation and breaks the IV dominance of the np pairing. The number of np pairs is increased by the attractive spin-triplet even TF, but the repulsive TF in the spin-triplet odd channel sometimes reduces the number of pairs as shown in Figs. 1, 3, and 5. For the ^{16}O case in Fig. 2, the IV dominance is rarely changed by the TF while the number of np pairs suddenly increases around the $\beta_2 \approx 0.1$ region by the TF. THis means that the attractive spin-triplet even TF may increase the IV np pairing. Sometimes the repulsive TF from the isospin-triplet odd channel for the like pairing shows

up in the number of nn and pp pairs due to the j-orbit mixing in the Nilsson orbit, although it is rather small compared with the attractive spin-triplet even TF in the np pairing.

For the possible BEC condensation of the np pairing condensation, we also studied the effect of the IS pairing enhancement by increasing the effective IS np coupling constant for ^{20}Ne in Fig. 6. But the BEC feature was not discovered by the increase of the effective IS np coupling constant. Even the IS dominance on the np pairing and the increase of the number of np pairs, which appeared at $\beta_2 = 0.5$, was unaffected by the IS coupling enhancement. The TF effects are also shown to be inevitable to explain the two-nucleon knockout data, σ_{-nn}, σ_{-pp}, and σ_{-np} from the ^{12}C + ^{12}C reaction experiment as tabulated in Table III.

In conclusion, the TF due to the spin-triplet channel is shown to play important roles in the np pairing correlations in some light $N = Z$ nuclei, such as ^{12}C, ^{16}O, ^{20}Ne, and ^{32}S. The nuclear deformation turns out to be another key factor to determine the number of IS pairs reflecting the TF property. This implies that the number of pairs is sensitive to the TF as well as the deformation, and consequently the choice of feasible targets and reactions for the deuteron extraction should be carefully selected. It is beyond the present work to discuss how the microscopic TF in the nucleon-nucleon interaction inside nuclei affects the macroscopic deformation of the nuclei and vice versa. Nevertheless, the TF in the pairing interactions turns out to enable us to properly explain the two-nucleon knockout data.

Finally we note that the present mean-field approach based on the Woods-Saxon potential is not enough to properly explain static nuclear properties. More developed calculations such as *ab initio* shell-model approaches are necessary for further quantitative analysis of the TF effect on the pairing correlations. Energy dependence of the two-nucleon knockout reaction from ^{12}C also deserves to be studied in the modern nuclear reaction theory for further comprehensive discussion of the TF effect.

[1] H. Sagawa, C. L. Bai, and G. Colo, Phys. Scr. **91**, 083011 (2016).

[2] D. J. Rowe, *Nuclear Collective Motion* (World Scientific, Singapore, 2010).

[3] I. Bentley and S. Frauendorf, Phys. Rev. C **88**, 014322 (2013).

[4] K. Neergard, Phys. Rev. C **80**, 044313 (2009); **88**, 049901(E) (2013).

[5] R. Subedi *et al.*, Science **320**, 1476 (2008).

[6] O. Hen *et al.*, Science **346**, 616 (2014).

[7] M. Patsyuk, O. Hen, and E. Piasetzky, EPJ Web Conf. **204**, 01016 (2019).

[8] K. Hagino, H. Sagawa, J. Carbonell, and P. Schuck, Phys. Rev. Lett. **99**, 022506 (2007).

[9] M. Baldo, U. Lombardo, and P. Schuck, Phys. Rev. C **52**, 975 (1995).

[10] W. Satula, D. J. Dean, J. Gary, S. Mizutori, and W. Nazarewicz, Phys. Lett. B **407**, 103 (1997).

[11] W. Satula and R. Wyss, Phys. Rev. Lett. **86**, 4488 (2001); **87**, 052504 (2001).

[12] S. M. Lenzi and M. A. Bentley, Lect. Notes. Phys. **764**, 57 (2009).

[13] A. Aoki, T. Hatsuda, and N. Ishii, Prog. Theor. Phys. **123**, 89 (2010).

[14] Y. Urata, K. Hagino, and H. Sagawa, Phys. Rev. C **96**, 064311 (2017).

[15] R. N. Bernard and M. Anguiano, Nucl. Phys. A **953**, 32 (2016).

[16] Y. Suzuki, H. Nakada, and S. Miyahara, Phys. Rev. C **94**, 024343 (2016).

[17] T. Otsuka, T. Suzuki, R. Fujimoto, H. Grawe, and Y. Akaishi, Phys. Rev. Lett. **95**, 232502 (2005).

[18] I. Tanihata, Phys. Scr. T **152**, 014021 (2013).

[19] E. Ha, M.-K. Cheoun, and H. Sagawa, Phys. Rev. C **99**, 064304 (2019).

[20] S. Terashima *et al.*, Phys. Rev. Lett. **121**, 242501 (2018).

[21] R. Schiavilla, R. B. Wiringa, S. C. Pieper, and J. Carlson, Phys. Rev. Lett. **98**, 132501 (2007).

[22] A. Gezerlis, G. F. Bertsch, and Y. L. Luo, Phys. Rev. Lett. **106**, 252502 (2011).

[23] E. Ha, M.-K. Cheoun, and H. Sagawa, Phys. Rev. C **97**, 024320 (2018).

[24] E. Ha, M.-K. Cheoun, H. Sagawa, and W. Y. So, Phys. Rev. C **97**, 064322 (2018).

[25] H. Matsubara *et al.*, Phys. Rev. Lett. **115**, 102501 (2015).

[26] A. Goswami and L. S. Kisslinger, Phys. Rev. **140**, B26 (1965).

[27] A. L. Goodman, G. L. Struble, J. Bar-Touv, and A. Goswami, Phys. Rev. C **2**, 380 (1970).

[28] A. L. Goodman, Nucl. Phys. A **186**, 475 (1972).

[29] S. Cwiok *et al.*, Comput. Phys. Commun. **46**, 379 (1987).

[30] E. Ha and M.-K. Cheoun, Nucl. Phys. A **934**, 73 (2015).

[31] A. L. Goodman, Phys. Rev. C **58**, R3051 (1998).

[32] S. Raman, C. W. Nestor, Jr., and P. Tikkanen, At. Data Nucl. Data Tables **78**, 1 (2001).

[33] G. A. Lalazissis, S. Raman, and P. Ring, At. Data Nucl. Data Tables **71**, 1 (1999).

[34] P. Moller, A. J. Sierk, T. Ichikawa, and H. Sagawa, At. Data Nucl. Data Tables **109-110**, 1 (2016).

[35] N. J. Stone, At. Data Nucl. Data Tables **90**, 75 (2005).

[36] M. K. Cheoun, A. Bobyk, A. Faessler, F. Šimkovic, and G. Teneva, Nucl. Phys. A **561**, 74 (1993); **564**, 329 (1993); M. K. Cheoun, A. Faessler, F. Šimkovic, G. Teneva, and A. Bobyk, *ibid.* **587**, 301 (1995).

[37] W. J. Vermeer, M. T. Esat, J. A. Kuehner, R. H. Spear, A. M. Baxter, and S. Hinds, Phys. Lett. B **122**, 23 (1983).

[38] S. Kubono, M. H. Tanaka, M. Sugitani, K. Morita, H. Utsunomiya, M.-K. Tanaka, S. Shimoura, E. Takada, M. Fukada, and K. Takimoto, Phys. Rev. C **31**, 2082 (1985).

[39] R. Machleidt, K. Holinder and Ch. Elster, Phys. Rep. **149**, 1 (1987).

[40] K. Langanke, J. A. Maruhn, and S. E. Koonin, *Computational Nuclear Physics 2* (Springer-Verlag, Berlin, 1983).

[41] B. A. Brown, W. A. Richter, and B. H. Wildenthal, J. Phys. G: Nucl. Phys. **11**, 1191 (1985).

[42] F. Simkovic, C. C. Moustakidis, L. Pacearescu, and A. Faessler, Phys. Rev. C **68**, 054319 (2003).

[43] H. Sagawa, T. Suzuki, and M. Sasano, Phys. Rev. C **94**, 041303(R) (2016).

[44] H. T. Chen and A. Goswami, Phys. Lett. B **24**, 257 (1967).

[45] H. Sagawa and T. Suzuki, Phys. Rev. C **97**, 054333 (2018).

[46] D. M. Brink and R. A. Broglia, *Nuclear Superfluidity* (Cambridge University, Cambridge, England, 2005).

[47] J. M. Kidd, P. J. Lindstrom, H. J. Crawford, and G. Woods, Phys. Rev. C **37**, 2613 (1988).

[48] E. C. Simpson and J. A. Tostevin, Phys. Rev. C **83**, 014605 (2011).

[49] E. C. Simpson, P. Navratil, R. Roth, and J. A. Tostevin, Phys. Rev. C **86**, 054609 (2012).

[50] Y. Ayyad *et al.*, Phys. Rev. C **96**, 021303(R) (2017).

[51] N. Sandulescu and G. F. Bertsch, Phys. Rev. C **78**, 064318 (2008).

[52] B. R. Barrett, P. Navrátil, and J. P. Vary, Prog. Part. Nucl. Phys. **69**, 131 (2013).